IOP Publishing Journal of Micromechanics and Microengineering
J. Micromech. Microeng. **30** (2020) 115022 (12pp) https://doi.org/10.1088/1361-6439/abb8c2

# Volume-preserving strategies to improve the mixing efficiency of serpentine micromixers

**Sajad Razavi Bazaz[1,6], Amir Hossein Hazeri[2,6], Omid Rouhi[1], Ali Abouei Mehrizi[2], Dayong Jin[3,4] and Majid Ebrahimi Warkiani[1,3,5]**

[1] School of Biomedical Engineering, University of Technology Sydney, Sydney, New South Wales 2007, Australia
[2] Department of Life Sciences Engineering, Faculty of New Sciences and Technologies, University of Tehran, Tehran, Iran
[3] Institute for Biomedical Materials and Devices, Faculty of Science, University of Technology Sydney, NSW 2007, Australia
[4] ARC Research Hub for Integrated Device for End-user Analysis at Low-levels (IDEAL), Faculty of Science, University of Technology Sydney, New South Wales 2007, Australia
[5] Institute of Molecular Medicine, Sechenov University, Moscow 119991, Russia

E-mail: majid.warkiani@uts.edu.au

Received 24 May 2020, revised 17 August 2020
Accepted for publication 15 September 2020
Published 30 September 2020

**Abstract**

In this study, we have proposed volume-preserving strategies to boost chaoticadvection and improve the mixing efficiency of serpentine micromixers. The proposed strategies revolve around the point that the volume of the micromixer is kept constant during the manipulation. The first strategy involves the utilization of a nozzle-diffuser (ND) shaped microchannel. Using this, the velocity of the fluids fluctuates in an alternating pattern, leading to additional chaotic advection, a decrease in the mixing path, and an increase in the mixing index. The second strategy uses non-aligned inlets to generate swirl inducing effects at the microchannel entrance, where the collision of two fluids generates angular momentum in the flow, providing more chaotic advection. These strategies proved to be effective in boosting the mixing efficiency over wide ranges of Re in which 60% enhancement (from 20.53% to 80.31%) was achieved for Re of 30 by applying an ND shaped microchannel, and 20% enhancement (from 12.71% to 32.21%) was achieved for a critical Re of 15 by applying both of the strategies simultaneously.

Supplementary material for this article is available online

Keywords: microfluidics, micromixer, serpentine microchannel, computational fluid dynamics, nozzle-diffuser shaped microchannels, non-aligned inlets

(Some figures may appear in colour only in the online journal)

## 1. Introduction

Microfluidics has progressed significantly in recent years, primarily due to the interest it has garnered from several fields [1] where numerous industries in the realms of biomedical, chemical, and pharmaceutical applications stand to benefit from this technology, defined as the manipulation of fluids at the microscale within a closed microchannel [2]. These minute platforms offer superior advantages over conventional macroscale approaches, including high levels of sensitivity, low-cost, user-friendliness, and low sample consumption [3, 4]. Along with the tremendous progress made in microfluidic techniques, the scope of microfluidic applications continues

[6] These authors contributed equally as first author.

 

to broaden, encompassing operations such as drug delivery, synthesis of nucleic acids, cell lysis, polymerase chain reaction, chemistry, and protein crystallization [5–8]. The most widely used microfluidic devices are micromixers [9, 10] droplet generators [11, 12], and particle/cell separators [13–17]. In many microfluidic operations, it is common for fluids to require mixing before moving on to downstream analysis; however, the Reynolds numbers (Re) in these micromixers are typically low. As a result, diffusion is the predominant mixing mechanism, and the mixing process is inherently slow. Despite this, micromixers remain one of the most important and principal components of lab-on-a-chip systems.

Micromixers are broadly divided into the two categories of passive and active [18]. Active micromixers require external forces such as thermal, acoustic, and magnetic fields for generating disturbance within the fluid to increase the mixing efficiency. However, these external fields may impose detrimental effects on biological samples. Moreover, the difficulty in their integration with lab-on-a-chip systems hampers their widespread utility. On the other hand, passive micromixers largely rely on chaotic advection by geometry manipulation, or diffusion by flow lamination, making them a more commercially viable option [19, 20]. These micromixers can readily be incorporated into the lab-on-a-chip devices with minimum cost and better reliability. Passive micromixers can be characterized into different groups based on the mixing mechanism, including chaotic advection, split and recombine, and lamination [21].

Micromixers can be further classified according to their effective Re; current micromixers are categorized into the three classes of high Re ($Re > 100$), intermediate Re ($10 < Re < 100$), and low Re ($Re < 10$) [22]. The operation of a micromixer largely depends on the nature of the experiment, where fluidic mixing within the inertial regime happens at high Re, while biological applications often require low Re (i.e. to give enough incubation time to samples for effective reaction). As such, a versatile micromixer capable of high mixing efficiency in a wide range of Re is desirable.

Passive micromixers have been extensively investigated for many microfluidic applications. These devices mainly fall into the planar and 3D micromixer classifications. Although 3D micromixers have relative high mixing efficiencies, some challenges arise around their integration with other parts of lab-on-a-chip devices and fabrication processes. Thus, planar micromixers have received far more attention and popularity. Reviewing the geometry of planar micromixers reveals that staggered herringbone structures are extremely popular within their class [23]. Inspired from transverse effects in micropatterned geometries [24], Strook and his colleagues proposed the first chaotic staggered herringbone mixer to enhance mixing efficiency in a straight microchannel [25]. However, these channels require a big footprint, and the channel is usually lengthened to properly exploit the effect of generated vortices. To address this issue, serpentine microchannels were proposed to enhance the mixing efficiency of two or more fluids within a small footprint. Serpentine micromixers such as the zig-zag, square-wave (SW), curved shaped, or multi-wave shaped microchannels are now well-known. Comprehensive studies for analyzing serpentine microchannels [26–28] reveal that SW microchannels are more efficient than other types, including zig-zag, curved, and multi-wave. The reason behind this is that these SW channels have more sharp turns and longer lengths compared to other serpentine channels. However, the mixing efficiency of these channels is not high at moderate flow rates, where most biological experiments occur. To meet this demand, the addition of mixing units and increasing the dimensions of the design were proposed as a solution to boost the mixing efficiency of an SW micromixer [26]. However, this method made a more volume-consuming device due to the enhancement of total length of the micromixer, requiring additional build materials and bigger footprint. In addition, using sinusoidal side walls for an SW microchannel, a higher mixing index compared to the simple SW microchannel was achieved [29]. Nonetheless, this approach resulted in more total length of the micromixer duo to using sinusoidal paths instead of straight paths. As the width and depth of the simple SW microchannel did not change after the manipulation, like the previously mentioned study, the volume of the first device was not kept constant. Moreover, a topology optimization approach based on maximizing the reverse flow SW channel was applied [30]. Nevertheless, the high aspect ratio made at the region of the manipulation could result in obtaining difficulties in the fabrication process. Also, various 3D serpentine microchannels have been proposed [31–33]. Despite the high mixing efficiency, the channel fabrication was troublesome, required cleanroom facility and adroit use, and often involved multi-step softlithography. Nevertheless, applying non-aligned inlets into a planar micromixer can result in a 3D micromixer, improving the performance of the planar micromixer and providing functional integration in microfluidic systems without any complexity in fabrication [34, 35].

In this study, strategies keeping the volume of the base geometry constant (volume-preserving), assisting in boosting chaotic advection were used to improve greatly the mixing efficiency of two inlet fluids within a small footprint, requiring no additional build materials and without having challenges for integration with other parts of the lab-on-a-chip devices and fabrication processes. To achieve this, nozzle-diffuser (ND) shaped channels are applied to a typical SW micromixer. By applying ND modifications to the typical SW micromixer, the velocity of the fluids increases and decreases, alternately. This, in turn, induces additional chaotic advection and vortices to decrease the diffusion path required for enhanced mixing. The other strategy to boost the mixing efficiency is to use non-aligned inlets to generate swirl inducing effects at the entrance of the main microchannel. This misalignment results in a height difference at the inlets of the device, generation of angular momentum, and enhancement of chaotic advection. Lastly, the credibility of the numerical results is evaluated by comparison of the experimental and numerical results.

## 2. Materials and methods

### 2.1. Numerical simulations

In this study, simulations were carried out via COMSOL Multiphysics 5.3a, a commercial software based on the finite element method [36]. All simulations were implemented by a desktop computer with Intel processor core i7-3610QM 2.30 GHz integrated with 8.00 GB RAM on a 64-bit operating system. The governing equations in this simulation are Continuity, Navier–Stokes, and Convection–Diffusion, as introduced in equations (1) to (3) [37]:

$$\nabla.V = 0 \tag{1}$$

$$\frac{\partial V}{\partial t} + \rho\left(V.\nabla\right)V = -\nabla P + \mu\nabla^2 V \tag{2}$$

$$\frac{\partial C}{\partial t} + \left(V.\nabla\right)C = D\nabla^2 C \tag{3}$$

where $P$ represents the pressure, $V$ defines the velocity vector, $C$ identifies the species concentration, and $D$ is the diffusion coefficient. In order to evaluate flow behavior within the channel, $Re$ is used, which is the ratio between inertial and viscous force and is described via equation (4):

$$Re = \frac{\rho U D_h}{\mu}. \tag{4}$$

Here, $\rho$ states the density, $U$ demonstrates the average velocity, $\mu$ shows the dynamic viscosity, and $D_h$ represents the hydraulic diameter, the calculation of which is demonstrated by equation (5):

$$D_h = \frac{4A}{P} \tag{5}$$

where $A$ is the area of the cross-section, and $P$ is the wetted perimeter of the cross-section [38]. In this study, all reported Re values are evaluated at the inlet cross-section.

The fluid properties were considered similar to the properties of water at room temperature. Thus, incompressible and Newtonian flow with the density of 1000 kg $m^{-3}$ and the dynamic viscosity of 0.001 Pa.s was applied. Furthermore, during the numerical calculations, the flow was considered steady-state. Uniform velocity has been set to both inlets, and zero static pressure has been applied to the outlet. No-slip boundary condition has been assigned to the walls. For the simulation setting of the micromixer, each stream was considered deionized water, either of which was labeled with red and green dye, which their diffusivity was considered $1.0 \times 10^{-9}$ $m^2$ $s^{-1}$. The molar concentration (mol $m^{-3}$) of two species was set as 0 and 1 for inlets 1 and 2, respectively. As a result, the uniform mixing was obtained in the molar intensity of 0.5 for the two species at the end of the mixing process. In addition, a quantity called the mixing index ($MI$) was defined in order to evaluate the quality of mixing, which is calculated by equation (6):

$$MI = 1 - \sqrt{\frac{1}{n}\sum_{i=1}^{n}\left(\frac{k_i - \bar{k}}{\bar{k}}\right)^2} \tag{6}$$

where $n$ is total numbers of sample points, $k_i$ is the mole fraction over the cross-section of the outlet, and $\bar{k}$ is the average mole fraction that is 0.5 in this study. The values of $MI$ vary from 0 to 1 where $MI = 0$ indicates no mixing occurs during the process, whereas $MI = 1$ shows that complete mixing occurs during the process.

### 2.2. Dye preparation

Food coloring (Queen Fine Foods, Alderley, Queensland, Australia) for visualization of the mixing process was used for bright field imaging. 1 ml of each dye was diluted in 49 ml MACS® buffer (Miltenyi Biotec, Germany) (ratio 1:49). The MACS® buffer contains phosphate buffered saline, 2 mM ethylenediaminetetraacetic acid supplemented with 0.5% BSA, and 0.09% sodium azide.

### 2.3. Device fabrication and experimental setup

Microchannels were fabricated via a high-resolution DLP 3D printer (MiiCraft, Hsinchu, Taiwan), possessing XY printing area of 32 mm × 57 mm and Z printing area of 120 mm [39]. For this aim, the geometry was first designed in Solidworks 2016, a commercially available CAD drawing software and then exported as an .stl file suitable for the 3D printer. The file is then imported into the 3D printer software (MiiCraft 125, Version 4.01, MiiCraft Inc.) and then sliced with 10 $\mu$m slice thickness. After successful printing, the part was rinsed with IPA, post cured for 20 s, and bonded to a glass slide via a double-coated adhesive tape [40]. Brightfield images were captured via a high-speed CCD camera (DP80, Olympus, Tokyo, Japan) mounted on an inverted microscope (IX73, Olympus, Tokyo, Japan).

## 3. Results and discussion

### 3.1. Grid study

In numerical simulations, additional numerical diffusion can be made related to the numerical errors due to the discretization of connective terms for determining the concentration distribution. In order to perform accurate numerical simulations, it is crucial to verify the grid study. Although it is not possible to eliminate the numerical diffusion completely, the numerical errors can be minimized by increasing the order of the discretization [41] and the grid density [42]. Moreover, the grid size and quality directly correlate with the accuracy of the results and calculation speed. Although a coarse mesh (a small number of meshes) is conducive to more timely calculations, the quality of the results is compromised since only a small number of discrete points within the domain

are evaluated. On the other hand, a finer mesh (high number of meshes) confers highly accurate results at the cost of time. As such, a trade-off between the total number of meshes and the accuracy of results is required. In this study, an SW micromixer (adapted from [28]) with a total length of 3900 $\mu$m, width of 200 $\mu$m, and height of 200 $\mu$m, which was manipulated by applying ND-shaped channels, was evaluated in a wide range of Re numbers (figure S1 (available online at stacks.iop.org/JMM/30/115022/mmedia)). To minimize the numerical errors, second order of discretization (quadratic) was selected instead of the first order (linear) to solve the convection–diffusion equation. Here, 1759898 finer quadratic elements provide a sufficient level of accuracy for the numerical calculations.

### 3.2. Volume-preserving strategies

SW micromixers have been used extensively across a plethora of applications. These microchannels are usually adopted for extremely low (Stokes regime) or high Re studies but do not possess adequate mixing efficiencies over short channel lengths at moderate Re. Therefore, the extension of microchannels is required to achieve a satisfactory mixing efficiency. In this study, we have proposed strategies to enhance mixing efficiency of SW micromixers, keeping the total volume of the device constant, while the baseline of the base geometry does not change tangibly. As illustrated in figure 1, the baseline is defined as the path inside the geometry, indicating the SW pattern for the investigated geometry.

Two strategies have been employed to boost the mixing efficiency. The first strategy involves the application of an ND-shaped microchannel to replace conventional straight microchannels. This geometry was applied in such a way that the volume of a model SW micromixer was kept constant. The second strategy uses non-aligned inlets to generate swirl inducing effects at the entrance of the main microchannel. This misalignment results in a height difference at the inlets of the device, allowing the collision of inlet fluids to create an initial swirl flow in the microchannel, leading to the addition of extra chaotic advection. By using non-aligned inlets, the height of inlets is decreased from 100 $\mu$m to 50 $\mu$m, and in order to keep the volume of the geometry constant, the length of the inlets is increased. Figure 1 depicts these strategies.

*3.2.1. Nozzle-diffuser technique.* By using ND-shaped channels, the velocity of the fluids fluctuates in an alternating pattern. As a result, additional chaotic advection is generated in the fluid domain. This phenomenon leads to decreasing the mixing path and increasing the mixing index. Figures 1(A)–(D) illustrate how the geometry has been manipulated from the base SW geometry to obtain the new ND-shaped geometry. Both the width and height of the channels are 100 $\mu$m, while $H = 400$ $\mu$m, $L_c = 2000$ $\mu$m, $W = 100$ $\mu$m, $B = 100$ $\mu$m, $Pi = 560$ $\mu$m, $L_o = 100$ $\mu$m, and $L_e = 1800$ $\mu$m.

With consideration of three geometric constraints, the ND-shaped SW microchannel was uniquely obtained. Firstly, according to the design of the ND-shaped channels, the baseline of the base SW geometry can alter either considerably or slightly. If the baseline changes drastically, the SW pattern will not be served in the ND-shaped geometry. Therefore, in order to keep the baseline almost in the same shape to have a SW pattern, both deviation angles ($\alpha$, $\beta$, figure 1(C)) for the horizontal channels were considered to be equal. Also, for the vertical channels, the parameters *j/k* and *h/i* demonstrated in figure 1(C) were set as 1. Secondly, as the features about 20 $\mu$m can easily be fabricated with cost-effective fabrication methods, the smallest dimension in the design ($c$, figure 1(C)) was not allowed to be lower than 20 $\mu$m. Thirdly, as the key feature of the manipulation process, the volume of the base geometry did not change, leading to setting the deviation angles as 16 degrees. Hence, the investigated ND-shaped channel in this study was attained by keeping the volume (6.61E + 07 $\mu m^3$) constant with almost the same baseline compared to the base channel, while the smallest dimension equals 20 $\mu$m (figure 1(C)). The geometric proportions regarding the dimensions, acquired due to this manipulation are depicted in figure 1(D), highlighting changes in the cross-sectional area of the microchannels. The simulations were performed for Re number from 0.002 to 100, and mixing indexes were calculated at the outlet by applying equation (6). As shown in figure 2, the ND-shaped micromixer outperforms the SW micromixer when evaluating the mixing index across all ranges of Re number.

Moreover, by lowering $c$, the volume of the micromixer decreases. Therefore, the deviation angles have to increase to keep the volume constant. Also, it is self-evident that the lower value of $c$ and the higher value of deviation angles can set the stage for more enhancement of the mixing quality due to the more drastic fluctuations occurring in the flow's velocity. Therefore, decision-makers can select values lower than 20 $\mu$m to have better device performance, however, requiring more accurate fabrication methods, which can result in consuming more cost and time to fabricate the device.

For low Re, the average velocity is small enough that fluids have enough time to completely diffuse, whereas, for high Re, the mixing mainly occurs by advection. According to the results, the minimum mixing index occurs at a Re of 15 for the typical SW micromixer, indicating the critical Re [43]. Consequently, for Re lower than 15, the mixing mechanism is diffusive, and for the Re more than 15, the mixing mechanism is predominantly advection. As previously described, the ND geometry creates more chaotic advection points inside the microchannel. Also, in serpentine microchannels and high Re, secondary flows exist, which further assist in the creation of chaotic advection within the channel. As a result, the effect of this geometry on the device's performance is more prevalent for Re higher than the critical Re. However, based on figure 2, this technique is able to improve the mixing efficiency of the channel even at Re lower than the critical Re where the diffusive mechanism is dominant.

To investigate the positive contributions of the ND geometry, the concentration, velocity, vorticity, and mixing index along the length of the microchannel are calculated numerically and presented in figure 3. Eight adjacent mixing units have been placed along the length of the ND-shaped SW

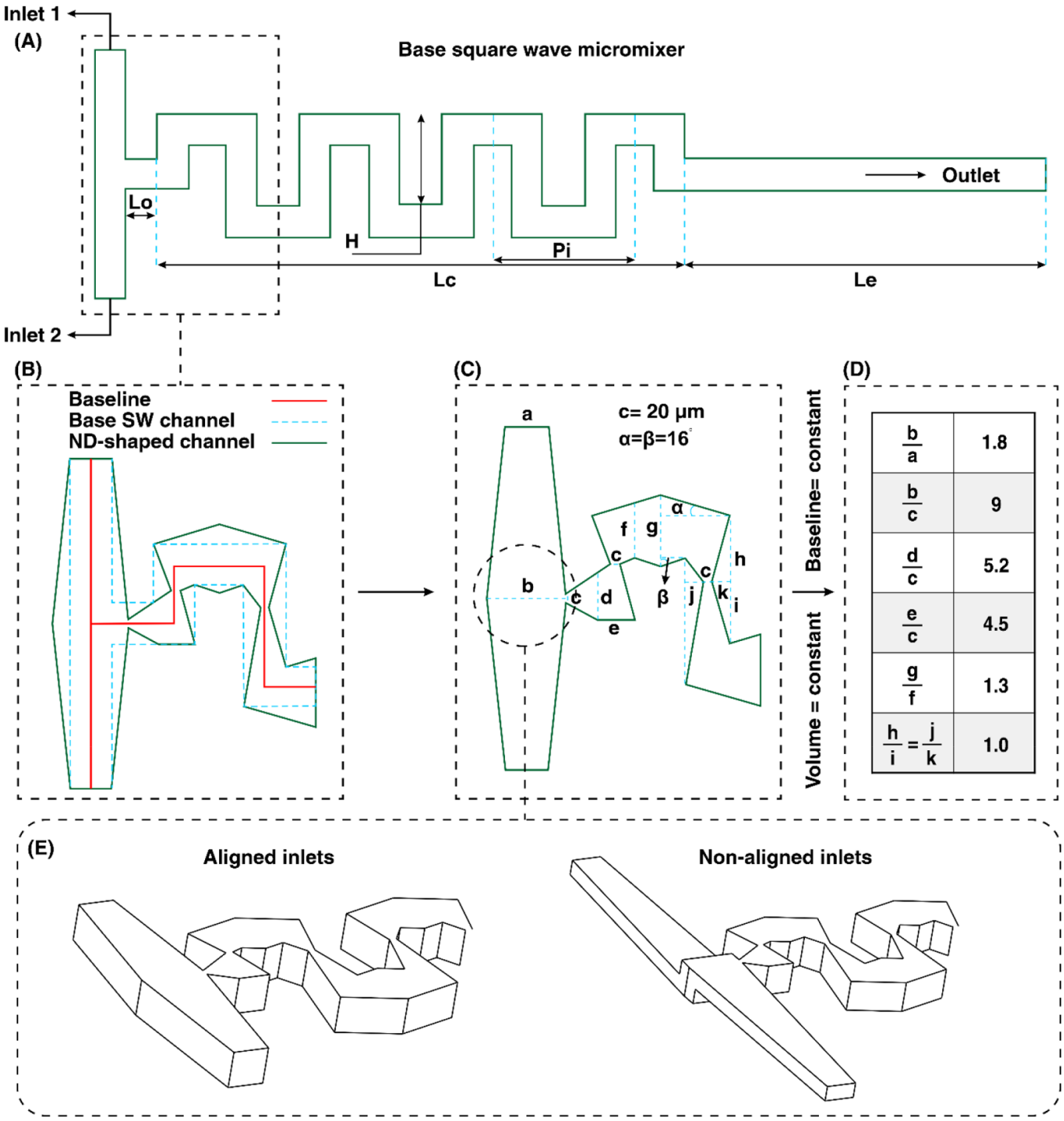


**Figure 1.** Strategies used to improve the mixing efficiency of an SW microchannel. (A)–(D) Manipulation process and parameters in order to transform an SW micromixer into an ND-shaped microchannel while keeping the volume and baseline constant. (E) Comparison between aligned and non-aligned inlets as a strategy to generate swirl inducing flow and increase chaotic advection. By using non-aligned inlets, their height is decreased, and in order to keep the volume of the geometry constant, the length of the inlets is increased.

micromixer which can be seen in figure 3(A). Figure 3(B) depicts the distributions of concentration, velocity, and vorticity along with different points in the microchannel (at the end of each mixing unit) and in three different Re. By using an ND geometry, additional chaotic advection inside the microchannel is created which is added to those generated by secondary flows in high Re regimes, and these cumulative effects assist in the enhancement of mixing index. For example, at a Re of 30, chaotic advection as a result of utilizing ND modifications dominates the flow regime and thus improves the quality of mixing. This advection mechanism along with the induced secondary flows helps to disturb the fluid stream, leading to a uniform concentration distribution at the outlet of the channel. Figure 3(C) illustrates the mixing index at the end of each

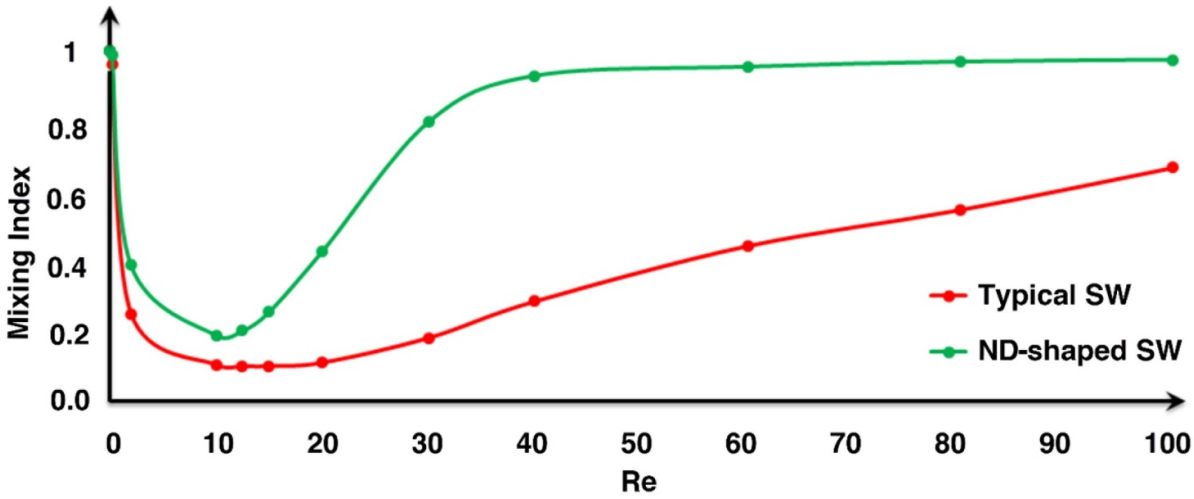


**Figure 2.** Comparison of mixing efficiency of an SW and ND-shaped micromixer. The results show outperforming of the ND-shaped micromixer to SW micromixer.

mixing unit, for the SW and ND-shaped micromixer, at Re of 2, 15, and 30. The ND-shaped micromixer generates a higher mixing index at each mixing unit in comparison with the typical SW geometry for all Re. Before applying the ND-shaped channels to the typical SW micromixer, among Re numbers of 2, 15 and 30, the highest mixing index is presented at a Re of 2 and the lowest at 15. This is due to the fact that the diffusion dominated flow regime at a low velocity affords more time for mixing at a Re of 2 than 15. Furthermore, the critical Re of 15 suffers from an insufficient incubation time as well as the absence of considerable chaotic advection inside the microchannel. However, after applying the ND-shaped channels into the typical SW micromixer, the highest mixing index for the design emerges at Re of 30 (figure S2). The magnitude of improvement in advective mixing as a result of the ND modifications far exceeds that seen in the diffusive range. This trend can be observed in figure 3(D) where the comparison between Re across all mixing units highlights the jump in mixing indexes. In addition, the mixing index enhancement follows a general upwards trend along the microchannel due to the aggregation of chaotic advection along with each mixing unit (see figure S3 for comparison of pressure distribution along the channel length).

*3.2.2. Non-aligned inlets.* The second previously mentioned strategy means to improve mixing efficiency involves the use of non-aligned inlets. As aforementioned, using non-aligned inlets led to decreasing the height of inlets from 100 $\mu$m to 50 $\mu$m, requiring increasing the length of inlets to keep the volume of the device constant. By creating a height offset between inlets, the collision between inlet fluids generates angular momentum in the flow inside the microchannel, providing more chaotic advection, as reported before [44, 45]. Therefore, in addition to applying ND-shaped channels, we can further improve the mixing efficiency by utilizing non-aligned inlets. To investigate the effects of this addition, non-aligned input channels were applied to the ND-shaped SW geometry analyzed in section 3.2.1, and the mixing index was evaluated at the outlet for the critical Re for different offset inlets. The lengthened inlets initially had the maximum distance allowable from each other, leaving one inlet higher with respect to the other (displacement ($X$) of 0). From there, each inlet was vertically displaced in six steps by 10, 10, 5, 5, 10 and 10 $\mu$m respectively until the inlet positions became reversed ($X$ = 50 $\mu$m). For each displacement point within this process, the effect of the vertical vortices on the total mixing index was investigated, the results of which are depicted in figure 4. The results depicted indicate that at $X$ = 0 and $X$ = 50 $\mu$m the highest mixing index is obtained owning to the highest offset distance between the inlets. This is mostly related to the generation of larger initial swirling flow streams inside the microchannel, concerning the other tested displacement values. Furthermore, at $X$ = 25 $\mu$m the lowest mixing index is produced due to the lack of offset distance between the inlets. The lower the offset distance, the smaller the swirl flow, thereby decreasing the mixing index [46–48].

Applying the largest offset distance tested to generate large swirling flow streams at the inlets, we have demonstrated that it is possible to further improve the mixing efficiency of the ND-shaped micromixer. By leveraging phenomena, the mixing index shows a marked improvement from the conventional SW (12.71% to 32.21% at Re 15) and a moderate improvement from the ND modified SW micromixer (27.85% to 32.21% at Re 15). By applying non-aligned inlets to the ND-shaped SW micromixer, the mixing index is elevated to 32.21% at the critical Re. Hence, although advection is not the main mechanism of the mixing process in the critical Re, by using these two proposed techniques, the mixing index was improved by 20%, ideal for applications where high mixing efficiency is essential.

Figure 5(A) shows streamlines at the cross-section of the collision between the inlet fluids of the ND-shaped SW micromixer, before and after applying the non-aligned inlets, at Re of 2 and 60. As it is depicted, in the Re of 2 for the ND-shaped SW micromixer, before applying the non-aligned inlets, no swirl flow is obtained. However, after adding the non-aligned

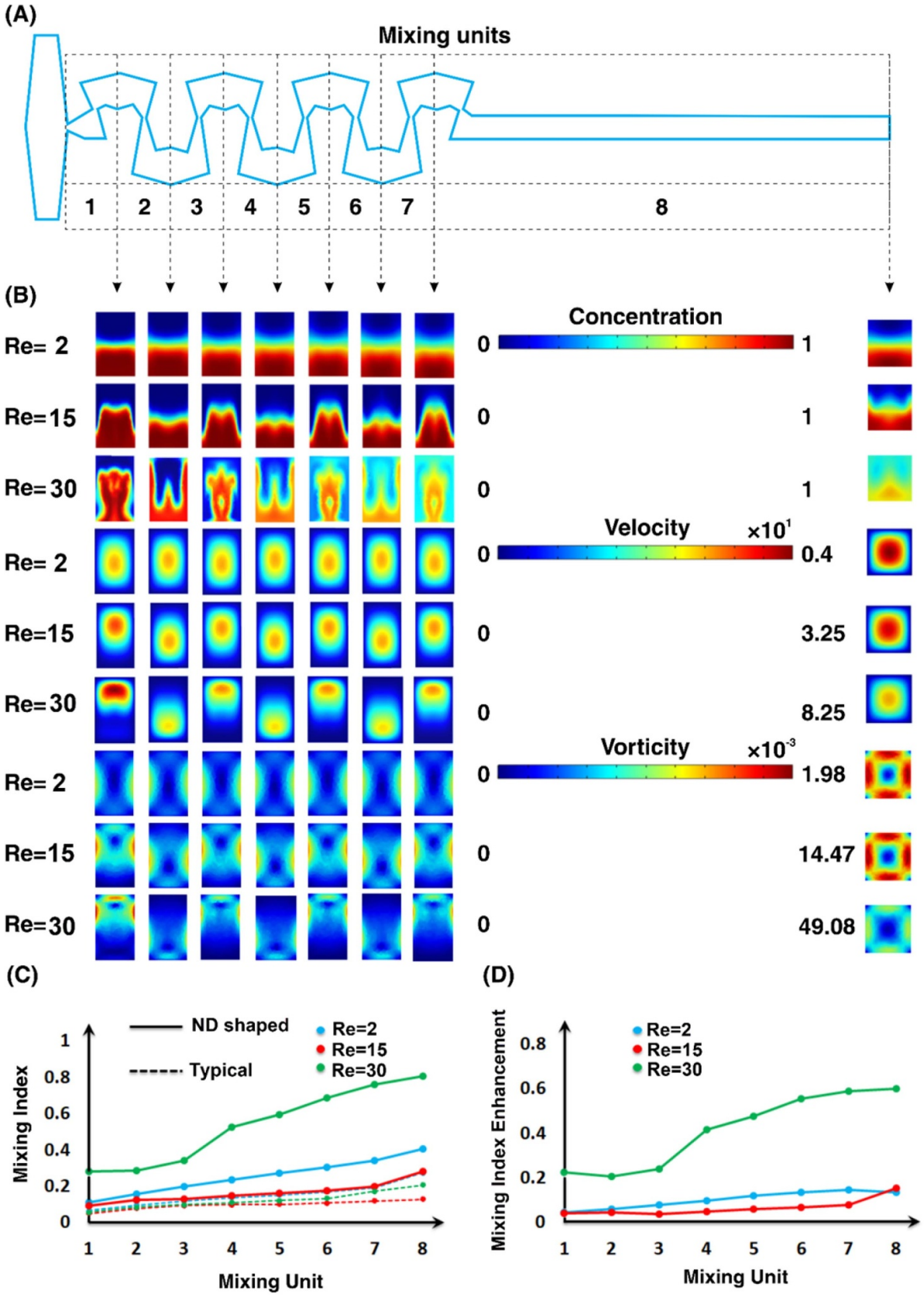


**Figure 3.** (A) Various mixing units along the length of ND-shaped microchannel. (B) Distribution of concentration, velocity, and vorticity for three Re of 2, 15, and 30. Investigation of (C) mixing index and (D) mixing index enhancement for different mixing units within an ND-shaped micromixer.

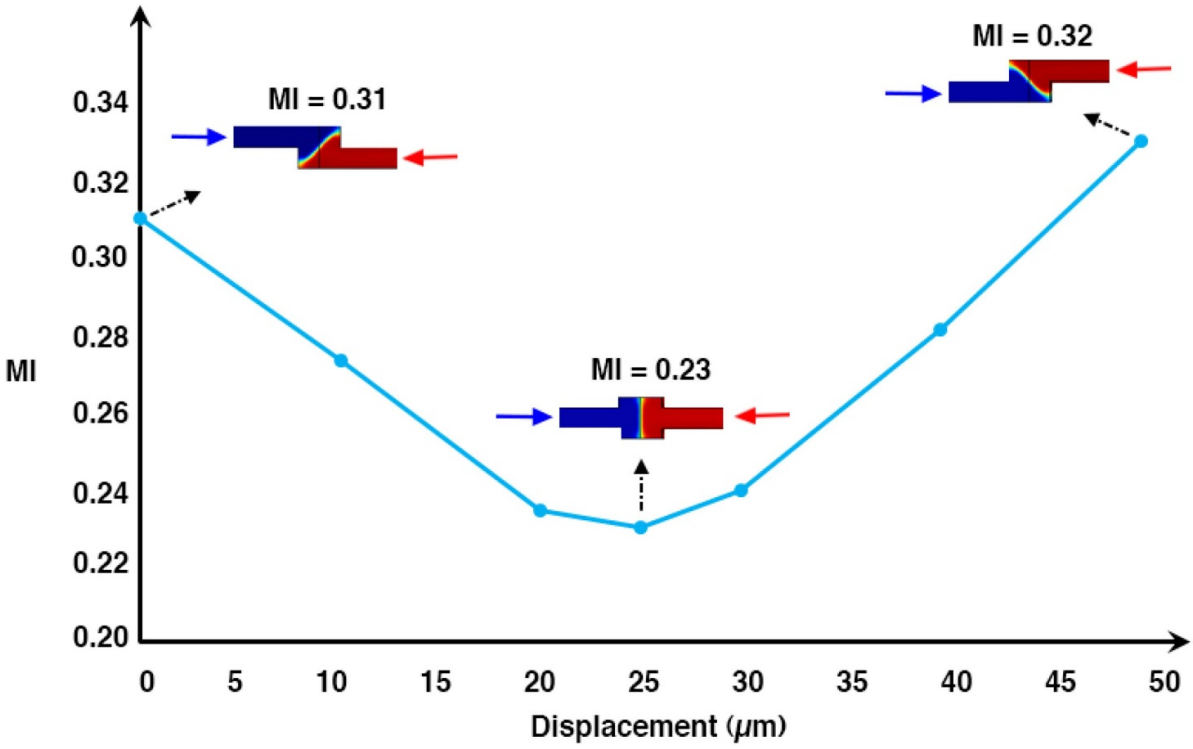


**Figure 4.** Mixing index at the different distances between inlets in critical Re number.

inlets, the dominated flow regime is changed and an anti-symmetric couple of counter-rotating vortices are observed. Accordingly, mixing quality is enhanced due to the additional chaotic advection inside the microchannel (figure S4). This effect becomes more pronounced when Re increases to 60, which is conducive to more improvement in the mixing index.

In order to better comprehend the effect of the swirl-inducing inlets combined with ND geometries, figures 5(B)–(E) show the velocity vectors at the cross-section of two different mixing units for the typical SW micromixer and ND-shaped SW micromixer with offset inlets at the critical Re. No vortex flow is created for the typical SW micromixer at the critical Re, while by applying ND-shaped channels and offset inlets into the typical geometry, vortex flow is generated (figures 5(A), (B)). Furthermore, the same effect is demonstrated for a Re of 60 in figures 5(C), (D). Although the higher Re induced vortices and secondary flows (owning to SW shape of the channel) inside the microchannel, by concurrently incorporating ND-shaped channels and non-aligned inlets into the typical geometry, the formation concentration of the vortex flow increases. As a result, more chaotic advection is induced within the microchannel while maintaining the total volume of the base SW microchannel.

*3.2.3. Scaling up the typical and ND shaped SW geometries.* While the improvements resulting from the application of an ND geometry have been demonstrated at one particular volume, many applications (particularly biological ones) may require larger channel volumes [49]. In applications where time is a limiting factor, dilutions are required, or larger particles are being used, larger channel cross-sections may be favorable. Therefore, in order to prove the effectiveness of our SW modification at a different scale, we aimed to observe the potential improvements of ND shapes on a larger SW micromixer.

The typical SW geometry was scaled up by multiplying by a factor of 5. The manipulation processes of applying ND-shaped channels into the scaled typical SW geometry are as same as what was shown in figures 1(A)–(D), and the difference only relies on the dimensions which are increased by the multiplying factor of 5. Both the width and height of the channels are 500 $\mu$m. Other dimensions are as follows: $H = 2000$ $\mu$m, $Lc = 10\,000$ $\mu$m, $Pi = 2800$ $\mu$m, $Lo = 500$ $\mu$m, and $Le = 9000$ $\mu$m. Simulations were performed for Re of 0.002 to 40. The results shown in figure 6(A) illustrate that even in an scaled-up geometry, the application of an ND geometry has a positive impact on the mixing efficiency. It can be seen that while the typical SW geometry relies upon the diffusion of fluid species across the laminar boundary, the upscaled ND-shaped SW micromixer is able to generate disturbance in the fluid boundary (figures 6(B), (C)). This demonstrates more efficient mixing over a shorter channel length, ideal for any application (see figure S5 for generalizing current strategies).

### *3.3. Experimental results*

In order to validate the credibility of our numerical results and calculations, a comparison between experimental and numerical results is mandatory. For the device fabrication, additive manufacturing, as a robust alternative method for softlithography was used [50]; this centered around the use of a high-resolution DLP 3D printer to directly print the microchannels

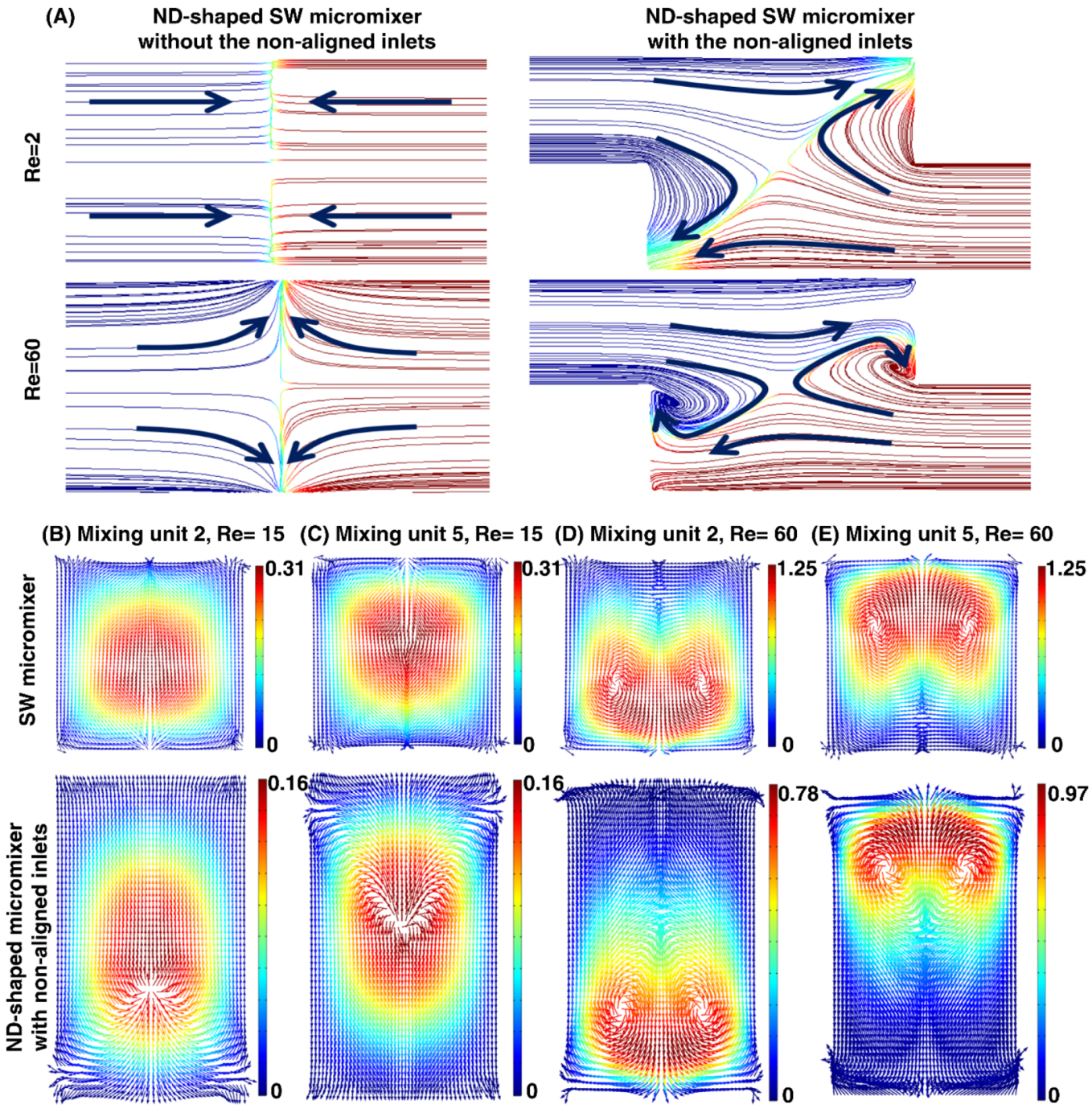


**Figure 5.** (A) Streamlines at the cross-section of the collision between the inlet fluids of the ND-shaped SW micromixer, before and after applying the non-aligned inlets, in the Re numbers of 1 and 30. Comparison of the velocity vectors and formation of the vortex flow inside the microchannel for SW micromixer and ND-shaped micromixer with non-aligned inlets for (B) mixing unit 2 and Re 1, (C) mixing unit 5 and Re 1, (D) mixing unit 2 and Re 30, and (E) mixing unit 5 and Re 30.

[51, 52]. To conveniently observe the microchannel and better capture the variation in concentration profile, a scaled-up micromixer was selected, designed, and fabricated. Two different diluted color dyes (red a green) were used as samples to be injected through the channel by a programmable syringe pump (Fusion 200, Chemics Inc.), and the results were captured by a high-speed CCD camera. Figure 7 shows the comparison between numerical and experimental results for two different Re of 3.6 (figure 7(A)) and 28.4 (figure 7(B)). Upon comparison, a reliable correlation between experimental and numerical results observed, confirming that numerical results can effectively predict the flow behavior inside the channel. Furthermore, image-based techniques were used to evaluate the credibility of numerical simulations and compare the values of mixing index obtained via numerical simulations and experimental process. To investigate the images quantitatively, grayscale values of the gray-scaled images were obtained by processing the chromatic images in the

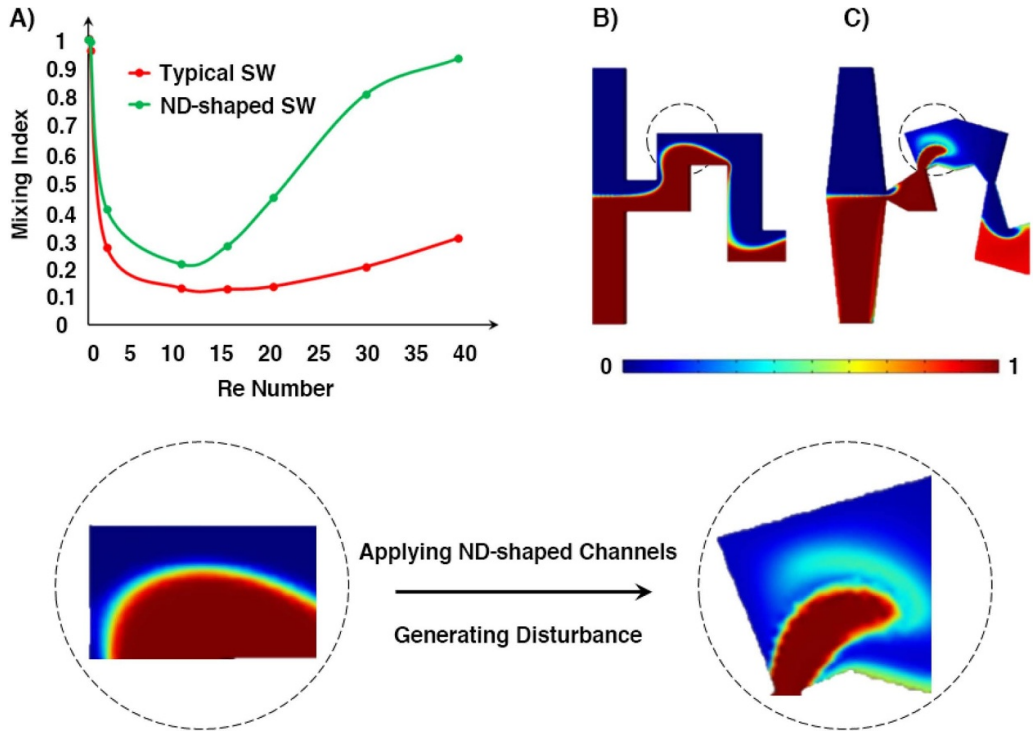


**Figure 6.** (A) Comparison between the mixing index of the scaled typical SW micromixer and the scaled ND-shaped micromixer. Comparison between the concentration distribution of (B) the scaled typical SW micromixer and (C) the scaled ND-shaped micromixer for Re 15.

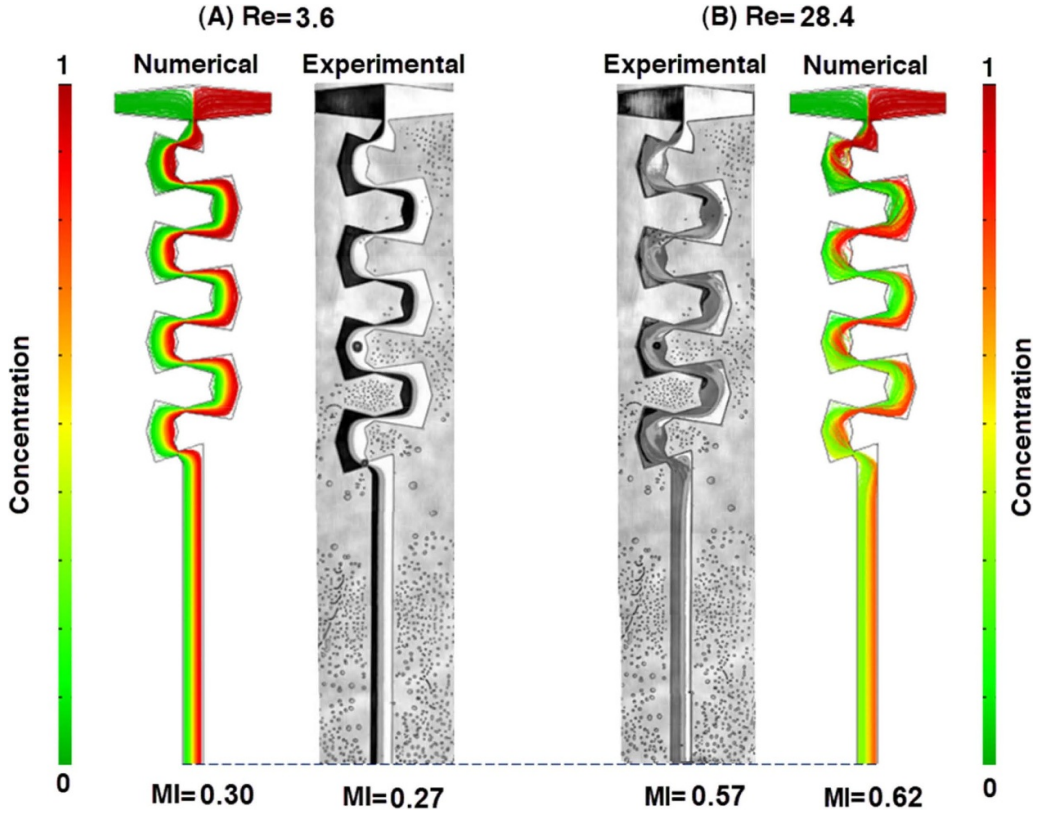


**Figure 7.** Comparison of experimental and simulation results regarding concentration distribution. In the sectional view, the level of mixing in both numerical and experimental results was compared for Re of (A) 3.6 and (B) 28.4, and the experimental results approved the credibility of numerical calculations.

Adobe Photoshop CC 2019 software, as the green color was set as black with grayscale value of 0 (normalized grayscale value of 0), and the red color was set as white with grayscale value of 255 (normalized grayscale value of 1). Then, a Matlab R2017a M-file code was written to obtain the normalized grayscale values of the images. Therefore, the grayscale values of the images were calibrated as the normalized grayscale of each point of the images represented the corresponding concentrations. Finally, by using the calculated concentrations with COMSOL Multiphysics 5.3a software for the numerical simulations, and image processing for the experimental images, mixing indexes at the outlet for the Re of 3.6 (figure 7(A)) and 28.4 (figure 7(B)) were evaluated by equation (6). The comparison between the numerical and experimental evaluations led to showing satisfactory results as the calculated mixing indexes were close to each other (less than 10% difference).

## 4. Conclusion

Serpentine micromixers were broadly utilized in a myriad of applications. These microchannels have a high mixing efficiency for extremely low and high-enough Re; however, they do not perform very well at moderate Re regimes. This study set out to propose and validate two novel strategies to boost the mixing efficiency of these channels while keeping the volume and baseline of the microchannel constant. With this aim, an SW microchannel as a candidate of serpentine microchannels was selected, and strategies to enhance their mixing were tested both numerically and experimentally. The first strategy was to utilize an ND-shaped microchannel for replacing conventional straight microchannels, generating additional chaotic advection inside the channel. The results showed that the mixing index of an SW micromixer reaches from 27.26% to 40.63%, 12.71% to 27.85%, and 20.53% to 80.31% at the Re numbers of 2, 15 and 30 respectively for an ND-shaped microchannel, indicating a significant improvement using this simple approach. The other strategy is to use offset inlets to generate swirl-inducing effect at the inlets which can propagate throughout the microchannel. Using offset inlets beside the ND-shaped channels led to improving the mixing index from 27.85% to 32.21% at the Re number of 15. Therefore, using the proposed strategies could lead to enhancing the mixing index about 20% at the critical Re number. Furthermore, the proposed ND technique was examined on a scaled micromixer, and the results show much improvement in the device performance. The findings of this study clearly indicate that these simple yet efficient strategies are beneficial for improving the mixing efficiency of serpentine micromixers. This can open up new avenues for researchers to design their desired micromixer with maximum efficiency and will be of broad use to the scientific, microfluidics, and biomedical communities. Also, serpentine microchannels have the capability of massive parallelization so that these devices can be used for processing of a large volume of samples.

## Acknowledgments

M E W would like to acknowledge the support of the Australian Research Council through Discovery Project Grants (DP170103704 and DP180103003) and the National Health and Medical Research Council through the Career Development Fellowship (APP1143377).

## ORCID iDs

Sajad Razavi Bazaz https://orcid.org/0000-0002-6419-3361
Omid Rouhi https://orcid.org/0000-0001-5905-6605
Majid Ebrahimi Warkiani https://orcid.org/0000-0002-4184-1944

## References

[1] Zhang J, Yan S, Yuan D, Alici G, Nguyen N-T, Warkiani M E and Li W 2016 Fundamentals and applications of inertial microfluidics: a review *Lab. Chip.* **16** 10–34
[2] Warkiani M E, Tay A K P, Guan G and Han J 2015 Membrane-less microfiltration using inertial microfluidics *Sci. Rep.* **5** 11018
[3] Hou H W, Warkiani M E, Khoo B L, Li Z R, Soo R A, Tan D S-W, Lim W-T, Han J, Bhagat A A S and Lim C T 2013 Isolation and retrieval of circulating tumor cells using centrifugal forces *Sci. Rep.* **3** 1259
[4] Kulasinghe A, Schmidt H, Perry C, Whitfield B, Kenny L, Nelson C, Warkiani M E and Punyadeera C 2018 A collective route to head and neck cancer metastasis *Sci. Rep.* **8** 746
[5] Sackmann E K, Fulton A L and Beebe D J 2014 The present and future role of microfluidics in biomedical research *Nature* **507** 181
[6] Streets A M and Huang Y 2013 Chip in a lab: microfluidics for next generation life science research *Biomicrofluidics* **7** 011302
[7] Mollajan M, Bazaz S R and Mehrizi A A 2018 A thoroughgoing design of a rapid-cycle microfluidic droplet-based PCR device to amplify rare DNA strands *J. Appl. Fluid Mech.* **11** 21–9
[8] Mahmoudi Z *et al* 2019 Promoted chondrogenesis of hMCSs with controlled release of TGF-β3 via microfluidics synthesized alginate nanogels *Carbohydr. Polym.* **229** 115551
[9] Rasouli M, Mehrizi A A, Goharimanesh M, Lashkaripour A and Bazaz S R 2018 Multi-criteria optimization of curved and baffle-embedded micromixers for bio-applications *Chem. Eng. Process.* **132** 175-86
[10] Kanaris A G, Stogiannis I A, Mouza A A and Kandlikar S G 2015 Comparing the mixing performance of common types of chaotic micromixers: a numerical study *Heat Transfer Eng.* **36** 1122–31
[11] Lashkaripour A, Mehrizi A A, Goharimanesh M, Rasouli M and Bazaz S R 2018 Size-controlled droplet generation in a microfluidic device for rare dna amplification by optimizing its effective parameters *J. Mech. Med. Biol.* **18** 1850002
[12] Lashkaripour A, Rodriguez C, Ortiz L and Densmore D 2019 Performance tuning of microfluidic flow-focusing droplet generators *Lab. Chip.* **19** 1041-53
[13] Condina M R, Dilmetz B A, Bazaz S R, Meneses J, Warkiani M E and Hoffmann P 2019 Rapid separation and identification of beer spoilage bacteria by inertial

microfluidics and MALDI-TOF mass spectrometry *Lab. Chip.* **19** 1961-70
[14] Kulasinghe A, Tran T H P, Blick T, O'Byrne K, Thompson E W, Warkiani M E, Nelson C, Kenny L and Punyadeera C 2017 Enrichment of circulating head and neck tumour cells using spiral microfluidic technology *Sci. Rep.* **7** 42517
[15] Aya-Bonilla C A *et al* 2017 Isolation and detection of circulating tumour cells from metastatic melanoma patients using a slanted spiral microfluidic device *Oncotarget* **8** 67355
[16] Raoufi M A, Mashhadian A, Niazmand H, Asadnia M, Razmjou A and Warkiani M E 2019 Experimental and numerical study of elasto-inertial focusing in straight channels *Biomicrofluidics* **13** 034103
[17] Razavi Bazaz S, Mashhadian A, Ehsani A, Saha S C, Krüger T and Ebrahimi Warkiani M 2020 Computational inertial microfluidics: a review *Lab. Chip.* **20** 1023–48
[18] Hessel V, Löwe H and Schönfeld F 2005 Micromixers—a review on passive and active mixing principles *Chem. Eng. Sci.* **60** 2479–501
[19] Chen X and Zhao Z 2017 Numerical investigation on layout optimization of obstacles in a three-dimensional passive micromixer *Anal. Chim. Acta* **964** 142–9
[20] Chen X, Zhang Z, Yi D and Hu Z 2017 Numerical studies on different two-dimensional micromixers basing on a fractal-like tree network *Microsyst. Technol.* **23** 755–63
[21] Lee C-Y, Wang W-T, Liu C-C and Fu L-M 2016 Passive mixers in microfluidic systems: a review *Chem. Eng. J.* **288** 146–60
[22] Nguyen N-T and Wu Z 2004 Micromixers—a review *J. Micromech. Microeng.* **15** R1
[23] Chen X and Wang X 2015 Optimized modular design and experiment for staggered herringbone chaotic micromixer *Int. J. Chem. React. Eng.* **13** 305–9
[24] Ajdari A 2001 Transverse electrokinetic and microfluidic effects in micropatterned channels: lubrication analysis for slab geometries *Phys. Rev.* E **65** 016301
[25] Stroock A D, Dertinger S K, Ajdari A, Mezić I, Stone H A and Whitesides G M 2002 Chaotic mixer for microchannels *Science* **295** 647–51
[26] Chen X, Li T and Hu Z 2017 A novel research on serpentine microchannels of passive micromixers *Microsyst. Technol.* **23** 2649–56
[27] Chen X, Li T, Zeng H, Hu Z and Fu B 2016 Numerical and experimental investigation on micromixers with serpentine microchannels *Int. J. Heat Mass Transf.* **98** 131–40
[28] Hossain S, Ansari M and Kim K-Y 2009 Evaluation of the mixing performance of three passive micromixers *Chem. Eng. J.* **150** 492–501
[29] Javaid M U, Cheema T A and Park C W 2018 Analysis of passive mixing in a serpentine microchannel with sinusoidal side walls *Micromachines* **9** 8
[30] Chen X and Li T 2016 A novel design for passive misscromixers based on topology optimization method *Biomed. Microdevices* **18** 57
[31] Malecha Z M and Malecha K 2014 Numerical analysis of mixing under low and high frequency pulsations at serpentine micromixers *Chem. Process Eng.* **35** 369–85
[32] Liu R H, Stremler M A, Sharp K V, Olsen M G, Santiago J G, Adrian R J, Aref H and Beebe D J 2000 Passive mixing in a three-dimensional serpentine microchannel *J. Microelectromech. Syst.* **9** 190–7
[33] Zhang H, Li X, Chuai R and Zhang Y 2019 Chaotic micromixer based on 3D horseshoe transformation *Micromachines* **10** 398
[34] Cortes-Quiroz C A, Azarbadegan A and Zangeneh M 2014 Evaluation of flow characteristics that give higher mixing performance in the 3-D T-mixer versus the typical T-mixer *Sensors Actuators* B **202** 1209–19
[35] Hossain S and Kim K-Y 2015 Mixing performance of a serpentine micromixer with non-aligned inputs *Micromachines* **6** 842–54
[36] Mashhadian A and Shamloo A 2019 Inertial microfluidics: a method for fast prediction of focusing pattern of particles in the cross section of the channel *Anal. Chim. Acta* **1083** 137-49
[37] Bazaz S R, Mehrizi A A, Ghorbani S, Vasilescu S, Asadnia M and Warkiani M E 2018 A hybrid micromixer with planar mixing units *RSC Adv.* **8** 33103–20
[38] Mahmoodi Z, Mohammadnejad J, Razavi Bazaz S, Abouei Mehrizi A, Ghiass M A, Saidijam M, Dinarvand R, Ebrahimi Warkiani M and Soleimani M 2019 A simple coating method of PDMS microchip with PTFE for synthesis of dexamethasone-encapsulated PLGA nanoparticles *Drug Deliv. Transl. Res.* **9** 707–20
[39] Razavi Bazaz S, Kashaninejad N, Azadi S, Patel K, Asadnia M, Jin D and Ebrahimi Warkiani M 2019 Rapid softlithography using 3D-printed molds *Adv. Mater. Technol.* **4** 1900425
[40] Razavi Bazaz S *et al* 2020 3D printing of inertial microfluidic devices *Sci. Rep.* **10** 5929
[41] Hardt S and Schönfeld F 2003 Laminar mixing in different interdigital micromixers: II. Numerical simulations *AIChE J.* **49** 578–84
[42] Ansari M A and Kim K-Y 2009 Parametric study on mixing of two fluids in a three-dimensional serpentine microchannel *Chem. Eng. J.* **146** 439–48
[43] Razavi Bazaz S *et al* 2020 Obstacle-free planar hybrid micromixer with low pressure drop *Microfluid. Nanofluidics* **24** 61
[44] Ansari M A, Kim K-Y, Anwar K and Kim S M 2012 Vortex micro T-mixer with non-aligned inputs *Chem. Eng. J.* **181** 846–50
[45] Ansari M A, Kim K-Y and Kim S M 2018 Numerical and experimental study on mixing performances of simple and vortex micro T-mixers *Micromachines* **9** 204
[46] Matsunaga T and Nishino K 2014 Swirl-inducing inlet for passive micromixers *RSC Adv.* **4** 824–9
[47] Cortes-Quiroz C, Azarbadegan A and Zangeneh M 2017 Effect of channel aspect ratio of 3-D T-mixer on flow patterns and convective mixing for a wide range of Reynolds number *Sensors Actuators* B **239** 1153–76
[48] Husain A, Khan F, Huda N and Ansari M 2018 Mixing performance of split-and-recombine micromixer with offset inlets *Microsyst. Technol.* **24** 1511–23
[49] Moloudi R, Oh S, Yang C, Teo K L, Lam A T L, Warkiani M E and Win Naing M 2019 Scaled-up inertial microfluidics: retention system for microcarrier-based suspension cultures *Biotechnol. J.* **14** 1800674
[50] Shrestha J, Ghadiri M, Shanmugavel M, Razavi Bazaz S, Vasilescu S, Ding L and Ebrahimi Warkiani M 2019 A rapidly prototyped lung-on-a-chip model using 3D-printed molds *Organs-on-a-Chip* **1** 100001
[51] Shallan A I, Smejkal P, Corban M, Guijt R M and Breadmore M C 2014 Cost-effective three-dimensional printing of visibly transparent microchips within minutes *Anal. Chem.* **86** 3124–30
[52] Vasilescu S A, Bazaz S R, Jin D, Shimoni O and Warkiani M E 2020 3D printing enables the rapid prototyping of modular microfluidic devices for particle conjugation *Appl. Mater. Today* **20** 100726